

The Northern Cross Fast Radio Burst project

IV. Multiwavelength study of the actively repeating FRB 20220912A

D. Pellicciari^{1,2}, G. Bernardi^{1,3,4}, M. Pilia⁵, G. Naldi¹, G. Maccaferri¹, F. Verrecchia^{14,15}, C. Casentini¹¹, M. Perri^{14,15},
F. Kirsten^{6,7}, G. Bianchi¹, C. Bortolotti¹, L. Bruno^{1,2}, D. Dallacasa^{1,2}, P. Esposito⁹, A. Geminardi^{5,9,10},
S. Giarratana^{1,2}, M. Giroletti¹, R. Lulli¹, A. Maccaferri¹, A. Magro¹¹, A. Mattana¹, F. Perini¹, G. Pupillo¹, M. Roma¹,
M. Schiaffino¹, G. Setti^{1,2}, M. Tavani^{12,13}, M. Trudu⁵, and A. Zanichelli¹

¹ INAF-Istituto di Radio Astronomia (IRA), via Piero Gobetti 101, Bologna, Italy
e-mail: davide.pellicciari@inaf.it

² Dipartimento di Fisica e Astronomia, Università di Bologna, via Gobetti 93/2, 40129 Bologna, Italy

³ South African Radio Astronomy Observatory, Black River Park, 2 Fir Street, Observatory, Cape Town, 7925, South Africa

⁴ Department of Physics and Electronics, Rhodes University, PO Box 94, Makhanda, 6140, South Africa

⁵ INAF-Osservatorio Astronomico di Cagliari, via della Scienza 5, I-09047, Selargius (CA), Italy

⁶ Department of Space, Earth and Environment, Chalmers University of Technology, Onsala Space Observatory, 439 92, Onsala, Sweden

⁷ ASTRON, Netherlands Institute for Radio Astronomy, Oude Hoogeveensedijk 4, 7991 PD Dwingeloo, The Netherlands

⁸ INAF-Osservatorio di Astrofisica e Scienza dello Spazio di Bologna, via Piero Gobetti 93/3, 40129, Bologna, Italy

⁹ Scuola Universitaria Superiore IUSS Pavia, Piazza della Vittoria 15, 27100 Pavia, Italy

¹⁰ Department of Physics, University of Trento, via Sommarive 14, 38123 Povo (TN), Italy

¹¹ Institute of Space Sciences and Astronomy (ISSA), University of Malta, Msida, MSD 2080, Malta

¹² INAF/IAPS, via del Fosso del Cavaliere 100, I-00133 Roma (RM), Italy

¹³ Università degli Studi di Roma "Tor Vergata", via della Ricerca Scientifica 1, I-00133 Roma (RM), Italy

¹⁴ SSDC/ASI, via del Politecnico snc, I-00133 Roma (RM), Italy

¹⁵ INAF-Osservatorio Astronomico di Roma, via Frascati 33, 00078 Monte Porzio Catone (RM), Italy

XXX-XXX-XXX

ABSTRACT

Context. Fast radio bursts (FRBs) are energetic, millisecond-duration radio pulses observed at extragalactic distances and whose origin is still largely debated. A fraction of the FRB population have shown repeating bursts. It is still unclear whether these represent a distinct class of sources.

Aims. We investigate the bursting behaviour of FRB 20220912A, one of the most active repeating FRBs known. In particular, we focus on its burst energy distribution, linked to the source energetics, and its emission spectrum, the latter directly related to the underlying emission mechanism.

Methods. We monitored FRB 20220912A at 408 MHz with the Northern Cross radio telescope and at 1.4 GHz using the 32-m Medicina Grueff radio telescope. Additionally, we conducted 1.2 GHz observations taken with the upgraded-Giant Meter Wave Radio Telescope searching for a persistent radio source coincident with FRB 20220912A, and we present the first upper limits obtained from a monitoring in X and γ rays conducted with Swift and AGILE satellites.

Results. We report 16 new bursts from FRB 20220912A at 408 MHz during the period of time between October 16th 2022 and December 31st 2023. Their cumulative spectral energy distribution follows a power law with slope $\alpha_E = -1.5 \pm 0.3$ and we measure a repetition rate of $0.15 \pm 0.04 \text{ hr}^{-1}$ for bursts having fluence $\mathcal{F} \geq 20 \text{ Jy ms}$. Furthermore, we report no detections at 1.4 GHz during down to a fluence of $\mathcal{F} \geq 13 \text{ Jy ms}$. These non-detections imply an upper limit of $\beta < -2.3$, with β being the global spectral index of FRB 20220912A. This is inconsistent with positive β values found for the only two known cases in which an FRB has been detected in separate spectral bands. We find that FRB 20220912A has shown a decline of 4 orders of magnitude in its bursting activity at 1.4 GHz over a one year time scale compared to literature observations, while remaining active at 408 MHz. The cumulative spectral energy distribution shows a flattening for spectral energy $E_\nu \geq 10^{31} \text{ erg Hz}^{-1}$, a feature seen so far in other two hyperactive repeaters. In particular, we highlight a strong similarity between FRB 20220912A and FRB 20201124A, in both the energy and repetition rate range. We also confirm the co-location of a continuum radio source at 1.2 GHz having $240 \pm 36 \mu\text{Jy}$ centered at FRB 20220912A coordinates.

Conclusions. The strong similarity between FRB 20220912A's and FRB 20201124A's cumulative energy distributions indicate that bursts from these sources are generated via similar emission mechanisms. Our upper limit on β suggests that the spectrum of FRB 20220912A is intrinsically narrow band. Finally, we ascribe the origin of the continuum source we detected to star formation processes in the vicinity of the FRB source, given also a recent non detection of a persistent radio source at milliarcsecond scale.

Key words. Methods: observational – Methods: data analysis – stars: magnetars – Radio continuum: galaxies

1. Introduction

Significant observational and theoretical efforts have been made to understand the origin of fast radio bursts (FRBs; see Bailes 2022; Petroff et al. 2022; Zhang 2023, for recent reviews), millisecond-long radio flashes of extragalactic nature. Many models invoke magnetars (e.g. Duncan & Thompson 1992; Thompson & Duncan 1995), i.e. neutron stars (NSs) powered by the decay of strong ($10^{14} - 10^{16}$ G) magnetic fields, as FRB progenitors (Popov & Postnov 2013; Beloborodov 2020; Lyubarsky 2020; Lu et al. 2020; Bochenek et al. 2021; Sobacchi et al. 2022). This hypothesis is supported by the simultaneous detection of an FRB-like burst, FRB 20200428 (CHIME/FRB Collaboration et al. 2020; Bochenek et al. 2020), with an X-ray outburst from the Galactic magnetar SGR J1935+2154 (Mereghetti et al. 2020; Ridnaia et al. 2020; Li et al. 2021; Tavani et al. 2021).

Nowadays ~ 800 distinct FRB sources are known (CHIME/FRB Collaboration et al. 2021; Xu et al. 2023), most of them classified as one-off events. However, ~ 50 sources (so-called repeaters) have shown repeated emission (CHIME/FRB Collaboration et al. 2023), ruling out catastrophic events as their origin. It is unclear whether all FRB sources are repeating in nature, although bursts from repeaters are statistically wider in temporal width and narrower in bandwidth compared to one-off FRBs (Pleunis et al. 2021). An interesting feature that has emerged from very long monitoring of the two hyperactive repeaters FRB 2021102A (R1) and FRB 20201124A is the flattening of their burst energy distributions at the highest burst energies (Hewitt et al. 2022; Jahns et al. 2023; Kirsten et al. 2024). This suggests a possible link between repeating and non-repeating FRB sources (James et al. 2022a; Kirsten et al. 2024), the latter presenting a flat luminosity distribution (James et al. 2022b,a), and could potentially imply that the most energetic bursts are produced by a different emission mechanism compared to the less energetic ones.

Among repeaters, various differences are found, especially in their observed level of activity. Indeed, the burst rate of repeaters spans a wide range of values, ranging from less active sources, which can exhibit a burst rate as low as $\sim 10^{-3}$ hr $^{-1}$ (CHIME/FRB Collaboration et al. 2023) to the most active ones showing sporadic burst storms in which the repetition rate rises up to several hundreds of bursts per hour (Li et al. 2021; Nimmo et al. 2022; Xu et al. 2022; Zhang et al. 2022, 2023; Feng et al. 2023). On the other hand FRB 20180916B, up to now the only source showing periodic windows of activity (Pleunis et al. 2021; Pastor-Marazuela et al. 2021), has not shown burst storms, with its repetition rate consistent with originating from a Poissonian process (Sand et al. 2023).

Repeating FRBs have been observed with extremely narrow spectra (Kumar et al. 2021; Pastor-Marazuela et al. 2021; Pleunis et al. 2021; Zhou et al. 2022; Zhang et al. 2023; Sheikh et al. 2023), hindering a multi-band detection and a robust spectral index measurement, which is crucial to investigate the underlying FRB emission mechanism and to exclude progenitor models (e.g. Burke-Spolaor et al. 2016). However, some exceptions have been reported. Remarkably, a single burst from R1 has been simultaneously detected at 1.4 GHz and 3 GHz using the Arecibo radiotelescope and the Karl G. Jansky Very Large Array (VLA), respectively (Law et al. 2017). Assuming a power law spectrum $F(\nu) \propto \nu^\beta$, the authors obtained a spectral index of $\beta = 2.1$. However, the latter result is inconsistent with the non-detection at 4.8 GHz conducted simultaneously with the Effelsberg radio telescope (Law et al. 2017). Therefore, the authors concluded that a single power-law function was not a good description

for the broadband spectrum of the source. Furthermore, Chawla et al. (2020) reported a coincident detection of FRB 20180916B in adjacent frequency bands of the Robert C. Byrd Green Bank Telescope (GBT) (300 – 400 MHz) and the Canadian Hydrogen Intensity Mapping Experiment (CHIME) (400 – 600 MHz). In this case, the burst in the CHIME band is downward drifting into the GBT band. This effect, known as "sad trombone", is commonly observed in the morphology of repeater bursts (e.g. Hessels et al. 2019). In the same work, no bursts have been detected in the Low Frequency Array (LOFAR) 110 – 190 MHz band, implying a lower limit on the broadband spectral index $\beta > -1.0$. Finally, the simultaneous detection of FRB 200428 at 600 MHz (CHIME/FRB Collaboration et al. 2020) and 1.4 GHz (Bochenek et al. 2020) gives a rough power law broadband spectrum of $\beta \sim 1$. However, in this case the flux density measured by CHIME is poorly constrained, given that this has been a sidelobe detection.

The chance to observe FRBs more than once allowed in-depth studies of these elusive sources, and helped in their accurate association with host galaxies (e.g. Gordon et al. 2023). The milliarcsecond localisation precision achieved for some actively repeating FRBs (e.g. Marcote et al. 2022) allowed the intriguing discovery of persistent radio sources (PRSs). A PRS is spatially coincident with the FRB site, and it is characterized by high luminosity ($L_\nu > 10^{27}$ erg s $^{-1}$ Hz $^{-1}$, Law et al. 2017) and compactness (< 10 pc, Marcote et al. 2017), the latter being inconsistent with typical values inferred from star-formation processes. Up to now, only two confirmed PRSs are known, both being associated with two actively repeating FRBs: R1 (Chatterjee et al. 2017) and FRB 20190520B (R1-twin; Niu et al. 2022). These FRB sources are very similar in terms of burst activity, host galaxy properties (Niu et al. 2022) and very high rotation measures (RMs) (Michilli et al. 2018; Anna-Thomas et al. 2023). In terms of spectral energy distribution (SED), the known PRSs exhibit flat radio spectra, with a spectral index $\beta \sim -0.27$ for R1 (Marcote et al. 2017) and $\beta \sim -0.4$ for R1-twin (Niu et al. 2022; Bhandari et al. 2023). In particular, the SED of the PRS associated with R1 resembles the Crab (PSR B0531+21) pulsar wind nebula, but with a magnetic field three orders of magnitude stronger to match the implied energetics of the PRS (Resmi et al. 2021). For these reasons the concordance picture for the radio emission of PRSs is a strongly ionized wind nebula powered by a young actively flaring magnetar (Margalit & Metzger 2018). Interestingly, results from very long baseline interferometry (VLBI) observations of R1-twin are also consistent with a hypernebula powered by the accretion of a central compact binary system (Sridhar et al. 2024; Bhandari et al. 2023). A third putative PRS is the one associated with FRB 20201124A, another very active FRB source (e.g. Zhou et al. 2022). Observations conducted with the VLA revealed the presence of a persistent, extended radio source coincident with the FRB position (Piro et al. 2021). However, at milliarcsecond scale the same radiation is completely resolved out (Nimmo et al. 2022), ascribing the continuum radiation to extended star formation occurring in the near environment of the FRB (Piro et al. 2021).

In September 2022, CHIME (CHIME Collaboration et al. 2022) discovered FRB 20220912A, a repeating FRB source having dispersion measure (DM) of 219.46 pc cm $^{-3}$ (McKinven & CHIME/FRB Collaboration 2022), subsequently localized with arcsecond precision in the outskirts of a moderately star-forming, massive galaxy at redshift $z = 0.0771$ (Ravi et al. 2023). Bursts were detected at different frequencies, between 408 MHz and 2.3 GHz (see Zhang et al. 2023, and references therein), with a period of particularly high activity in which a burst rate

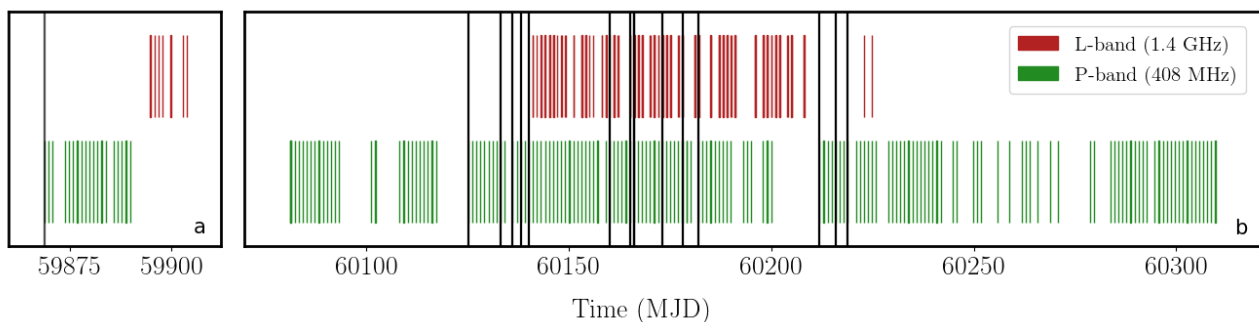


Fig. 1: Overview of the FRB 20220912A monitoring campaign. Panel *a* displays the MJD range 59868 – 59903 (35 days), while panel *b* shows the MJD range 60081 – 60309 (228 days). Green (red) vertical blocks indicate observations at 408 MHz (1.4 GHz). Vertical black lines represent burst detections at 408 MHz. Each observing session at 408 MHz last ~ 35 minutes, while 1.4 GHz observations started 15 minutes before the P-band run and last ~ 60 minutes.

of $\sim 400 \text{ hr}^{-1}$ were observed at 1.4 GHz (Feng et al. 2023; Zhang et al. 2023). A fraction of the observed bursts show very narrow-band spectra (Zhang et al. 2023) and short durations ($\sim 16 \mu\text{s}$), the latter usually clustered in dense burst forests (Hewitt et al. 2023a). No burst has been seen at frequencies higher than 2.3 GHz so far (Kirsten et al. 2022; Rajwade et al. 2022; Sheikh et al. 2022). The source was recently localised at RA (J2000) = $23^{\text{h}}09^{\text{m}}04.8988^{\text{s}} \pm 0.0003^{\text{s}}$, Dec (J2000) = $48^{\circ}42'23.908'' \pm 0.005''$ (Hewitt et al. 2023b), placing it closer to the centre of the host galaxy than previously suggested. Their observations also rule out the presence of a PRS down to a $\sim 20 \mu\text{Jy beam}^{-1}$ level. It was argued by Ravi et al. (2023) that the DM contribution by the host is low ($\leq 53 \text{ pc cm}^{-3}$). A low DM host contribution, along with an approximately zero rotation measure (RM) (McKinven & CHIME/FRB Collaboration 2022; Zhang et al. 2023; Feng et al. 2023; Hewitt et al. 2023a), corroborates the hypothesis of a clean local environment (Hewitt et al. 2023a).

In this work, we report the first multiwavelength monitoring campaign of FRB 20220912A, carried out at 408 MHz with the Northern Cross (NC) radio telescope, at 1.4 GHz with The Medicina Grueff 32-m single dish and at X and γ rays with the The Neil Gehrels Swift Observatory (Swift) (Gehrels et al. 2004) and AGILE (Tavani et al. 2009) satellites. Furthermore, we use new deep continuum radio observations taken with the upgraded Giant Meter Wave Radio Telescope (uGMRT) at band-5 (1.0 – 1.4 GHz) to investigate the presence of a PRS in the direction of FRB 20220912A.

The paper is structured as follows. In Section 2 we describe the multiwavelength campaign conducted on FRB 20220912A, in Section 3 we present and discuss the results of the observations and we draw our conclusions in Section 4.

2. Observations

2.1. Northern Cross Radio Telescope

The NC radio telescope is a T-shaped transit radio telescope deployed near Medicina (Italy). The telescope operates at 408 MHz (P-band) with a 16 MHz bandwidth, and it is undergoing an upgrade of the receiving system (Locatelli et al. 2020) to enable, amongst others, FRB observations. The current telescope configuration has two differences with respect to observations presented in Trudu et al. (2022) and Pellicciari et al. (2023). First, it doubles the collecting area, combining sixteen cylinders of the North-South arm into a single beam, whose half power beam width is now of $1.6^{\circ} \times 0.25^{\circ}$. Second, the delay correction needed

to form the beam is performed at higher cadence, i.e. every 5 s, effectively tracking the source across the field of view. Observations are stored to disk as 16-bits SIGPROC (Lorimer 2011) filterbank files, with a time resolution of $138.24 \mu\text{s}$ and a 14.468 kHz frequency channel width (see Locatelli et al. 2020, for a detailed description of the system).

We started monitoring FRB 20220912A with 8 cylinders on October 16th 2022, forming a single beam at the source coordinates, R.A. (J2000) = $23^{\text{h}}09^{\text{m}}04.9^{\text{s}}$, Dec (J2000) = $+48^{\circ}42'25.4''$ (Ravi et al. 2023). After the first 14-hrs on source, observations were interrupted and resumed on May 17th 2023, when 16 cylinders were employed. Observations ended on December 31st 2023, for a total of 122 hr on-source. Each session of observation lasted for ~ 35 min. As in Trudu et al. (2022) and Pellicciari et al. (2023), we performed a weekly calibration through interferometric observations of Cas A. A summary of the conducted observations is shown in Fig. 1.

2.2. Medicina Grueff Radio Telescope

Simultaneous observations were carried out at 1.4 GHz (L-band) with the Medicina Grueff 32 m dish (hereafter Medicina). The total duration of the campaign was 177 hours, made of ~ 1 hr daily runs. We recorded 2-bit baseband data in both circular polarizations written to disk in VDIF format (Whitney et al. 2010), using the local digital baseband converter (DBBC) system (Tucari 2003). Observations are centred at 1414 MHz, sampling a 128 MHz bandwidth divided into four separated sub-bands. Data were converted to filterbank format using a custom-built pipeline (Kirsten et al. 2020) and stored to disk with a 250 kHz frequency and $64 \mu\text{s}$ time resolution respectively. Two circular polarizations were averaged together to obtain total intensity data. The telescope has a system equivalent flux density (SEFD) of 458 Jy at 1.4 GHz, which leads, using the radiometer equation, to a $\sigma_L \approx 1.2 \text{ Jy ms}$ root mean square (rms) noise for a burst of 1 ms of duration. In order to test the data acquisition and conversion we observed PSR B0329+54, from which we successfully detected single pulses (Fig. 2).

2.3. uGMRT

In order to search for a PRS coincident to the position of FRB 20220912A, new continuum radio observations of FRB 20220912A were performed with the uGMRT in the 1050–1450 MHz (band-5) frequency range on UT 2023 November 1st. The

Table 1: Burst properties at 408 MHz from FRB 20220912A.

Burst ID	TOA (B.A.T.)	DM (pc cm ⁻³)	Width (ms)	F_{peak} (Jy)	\mathcal{F} (Jy ms)	E_{ν} (10 ³⁰ erg Hz ⁻¹)	E_i (10 ³⁷ erg)
B01	59868.885988115	219.6(5)	4.1(5)	18(1)	74(5)	12.3(7)	20(1)
B02	60125.160302085	220.2(3)	3.1(4)	7.4(6)	23(2)	3.8(3)	6.1(5)
B03	60133.142754625	220.1(2)	9.4(6)	4.3(4)	40(4)	6.7(5)	10.7(8)
B04	60136.132478465	219.6(4)	4.1(6)	6.8(6)	28(2)	4.6(4)	7.4(6)
B05	60138.120952875	219.7(6)	16(2)	4.8(3)	77(5)	12.8(7)	20(1)
B06	60140.121695755	220.4(2)	3.4(4)	7.6(6)	26(2)	4.3(3)	6.9(5)
B07	60160.070367215	220.1(2)	1.4(2)	9(1)	13(2)	2.1(3)	3.4(5)
B08	60165.061278865	219.4(3)	5.2(8)	7.3(6)	38(3)	6.3(5)	10.1(8)
B09	60166.045907535	219.9(2)	3.2(5)	6.2(6)	24(2)	3.3(4)	5.3(6)
B10	60166.045908315	219.7(2)	3.1(4)	5.5(7)	20(2)	2.8(3)	4.5(5)
B11	60173.031215725	221.3(5)	14.6(8)	10.1(3)	147(5)	24.5(6)	40(1)
B12	60178.024922305	220.1(4)	2.9(1)	29.9(7)	86(2)	14.4(3)	23.1(5)
B13	60182.006531445	220.2(2)	4.3(3)	13.3(6)	57(3)	9.5(4)	15.2(6)
B14	60211.931989265	220(1)	4.3(6)	4.9(5)	21(3)	3.5(4)	5.6(6)
B15	60215.918013385	220.8(4)	6.8(7)	6.5(4)	44(3)	7.3(5)	11.8(8)
B16	60218.898463655	223(1)	10(2)	3.8(4)	38(5)	6.3(8)	10(1)

Notes. Columns are, from left to right, the burst ID, the barycentric arrival time (B.A.T) at infinite frequency expressed as the modified Julian day (MJD), the fit-optimized DM, the full width at half maximum (FWHM) duration, the peak flux density, the fluence, the spectral energy and the isotropic burst energy, the latter computed multiplying the spectral energy for 16 MHz, i.e. the bandwidth used in NC observations.

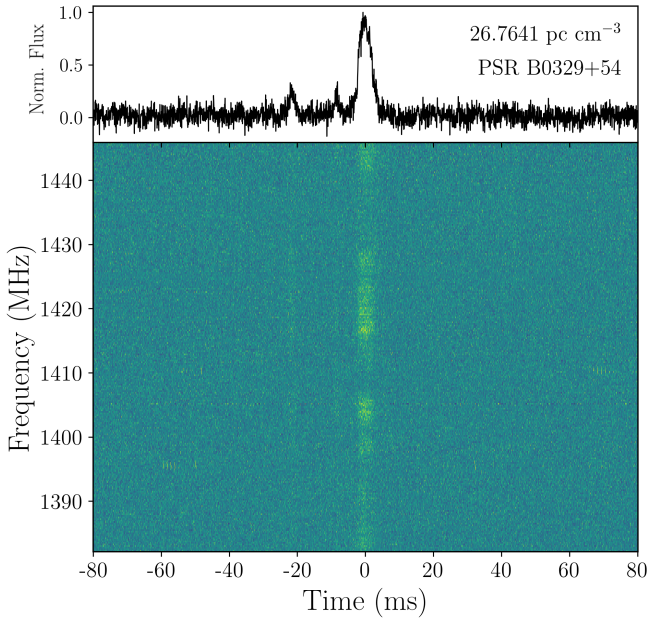


Fig. 2: Dynamical time-frequency plot of a single pulse from PSR B0329+54, detected at 1.4 GHz, using the Medicina Grueff radio telescope. The upper panel represents the frequency averaged time series. The DM at which the data are de-dispersed is reported in the upper right corner of the image.

total bandwidth is splitted into 16384 channels of 24.414 kHz each. The field of FRB 20220912A was observed for a total of ~ 3 hours. The sources 3C48 and J2322+509, a nearby source to the target, were used as absolute flux scale and phase calibrators, respectively.

The high spectral resolution of our data enabled us to split the total bandwidth in 8 sub-bands of 50 MHz each for easier data reduction. We processed each sub-band independently by carrying

out a standard interferometric data reduction¹ using the Common Astronomy Software Applications (CASA; McMullin et al. 2007) package. We iteratively performed flagging of RFI, band-pass, amplitude and phase calibrations for each sub-band. Finally, the calibrated visibilities of all the sub-bands were recombined for imaging. We assumed 3C48 to be 17.7 Jy at 1.2 GHz, with a spectral index $\beta = -0.76$ (Perley & Butler 2013). These measurements were used for the 3C48 flux and bandpass calibrations, which were then transferred to J2322+509. Finally, we determined gain and phase calibration for J2322+509 and then transferred them to the target field. Owing to severe RFI, two out of eight sub-bands were flagged, thus leaving 300 MHz of remaining bandwidth. Imaging was carried out with the TCLEAN task in CASA, by weighting the visibilities according to the briggs scheme with a ROBUST parameter -1 . We achieved a final noise level of $36 \mu\text{Jy beam}^{-1}$ at an angular resolution of $1.97'' \times 1.77''$.

2.4. Swift and AGILE monitoring

Since its discovery (McKinven & CHIME/FRB Collaboration 2022), FRB 20220912A has been added to the AGILE list of sources monitored during the Spinning-mode observations. We verified the source exposure with the MiniCalorimeter (MCAL; $0.4 \text{ MeV} \leq E \leq 100 \text{ MeV}$) detector and the Gamma-Ray Imaging Detector (GRID; $30 \text{ MeV} \leq E \leq 30 \text{ GeV}$). We take as each burst arrival time the de-dispersed topocentric arrival times at infinite frequencies. AGILE acquired MCAL data covering 3 of the 16 bursts presented here, due to South Atlantic Anomaly (SAA) passages or Earth occultation. We selected good events with standard selection criteria, such as the SAA passages time intervals exclusion, and inclusion of events with off-axis angles smaller than 60 degrees or at angles from Earth direction greater than 80 degrees.

A monitoring campaign with Swift has also started in fall 2022, similar to the one dedicated to FRB 20180916B (partially reported in Tavani et al. 2020; Trudu et al. 2023). Swift observed FRB 20220912A with the X-ray Telescope (XRT, Burrows et al.

¹ See <https://science.nrao.edu/facilities/vla/docs/manuals/obsguide/topical-guides/lofreq>

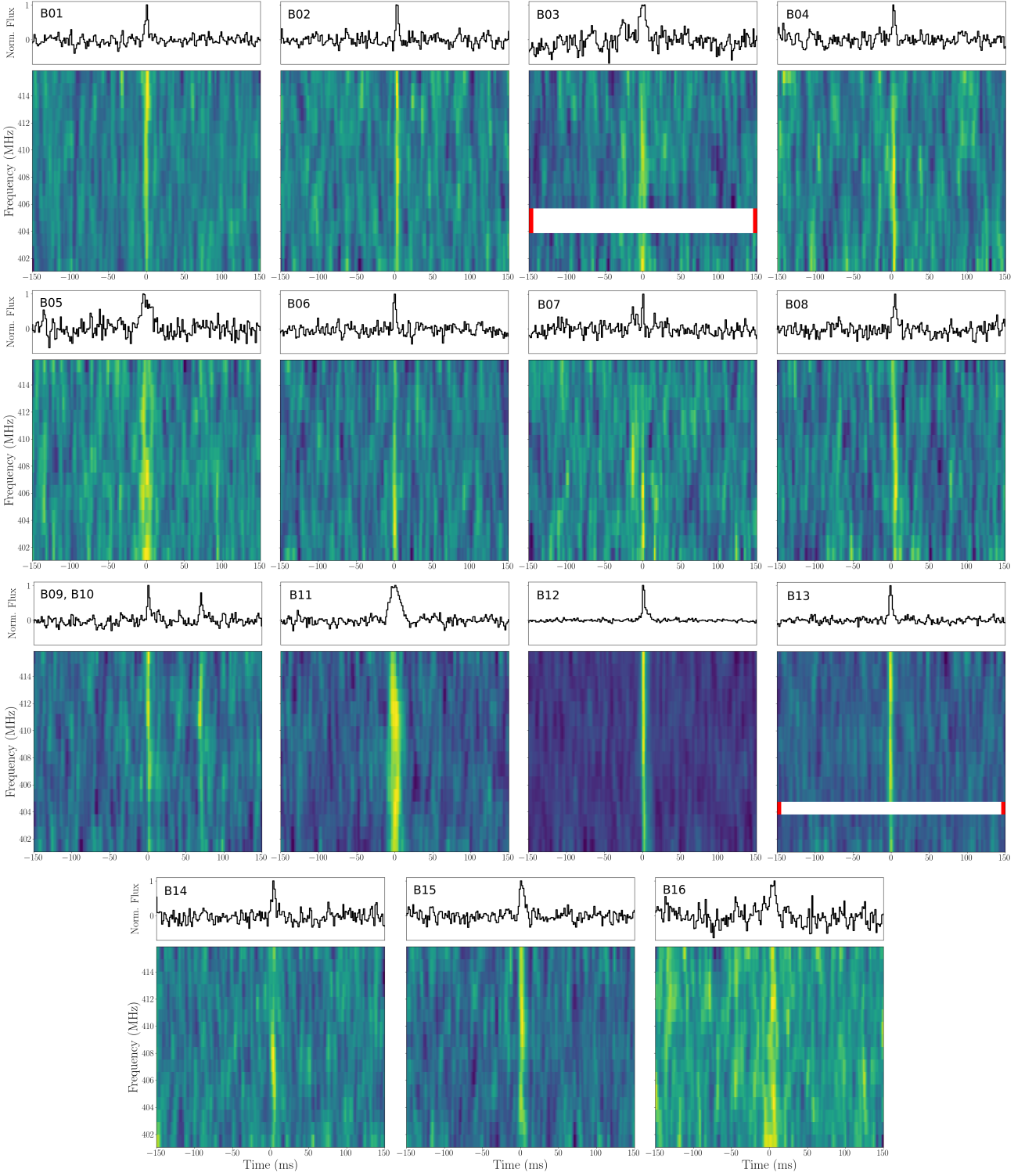


Fig. 3: Bursts from FRB 20220912A observed at 408 MHz. Both the de-dispersed, dynamic spectrum (bottom sub-panels) and the frequency-averaged profiles (top sub-panels) are shown. For a better visualisation, data were down-sampled to have 16 frequency channels, each 1 MHz wide, and time bins with 1.5 ms width. Horizontal white rows (highlighted with red ticks) are flagged channels due to RFI.

2005), one of the three instruments onboard. The Swift/XRT X-ray (0.3–10 keV) data were obtained daily after time of opportunity requests during source activity phases (on November 2022, and July–October, 2023, partially covering the radio monitoring presented in this work). The XRT observations were carried out in windowed timing (WT) readout mode, with 2–10 daily point-

ings. The time resolution of WT data is 1.8 ms and each pointing has a typical exposure of ~ 1.8 ks. We considered the combination of all the data and processed them using the XRTDAS software package (v.3.7.0)² within the HEASoft package (v.6.32.1).

² developed by the ASI Space Science Data Center (SSDC)

We cleaned and calibrated the data with standard filtering criteria using the `xrtpipeline` task and the calibration files available from the Swift/XRT CALDB (version 20230705). The imaging analysis was executed selecting events in the energy channels between 0.3 and 10 keV and within a 20 pixel ($\sim 47''$) radius, including the 90% of the point-spread function. The background was estimated from a nearby source-free circular region with the same radius value.

3. Results and discussion

The search for FRB candidates in NC data follows the strategy employed in [Trudu et al. \(2022\)](#) and [Pellicciari et al. \(2023\)](#), using the `SPANDAK` pipeline ([Gajjar et al. 2018](#)), which flags RFIs through `RFIFIND` ([Ransom et al. 2002](#)) and searches for single pulses with `HEIMDALL` ([Barsdell et al. 2012](#)). We considered a signal-to-noise ratio (S/N) greater than 8, a boxcar width shorter than 35 ms, and we searched using DM between 200 pc cm^{-3} and 240 pc cm^{-3} , given the nominal 220 pc cm^{-3} DM of the source. In the case of observations at 1.4 GHz, we set the threshold to be $S/N > 10$, in order to minimize the RFI contamination. In order to cross-check the results of the single-pulse search conducted at 1.4 GHz with the pipeline described above, we searched for FRBs in a large amount of data also with the processing pipeline described in [Kirsten et al. \(2021, 2024\)](#), which searches FRB with `HEIMDALL` and classifies bursts with the deep learning classifier `FETCH` ([Agarwal et al. 2020](#)).

We detected a total of 16 bursts at 408 MHz, and labeled them as “Bn”, ordered according to their time of arrival (ToA). We show their dynamic, de-dispersed spectra in Fig. 3, while their measured properties are reported in Table 1. All radio bursts, except for the first one, B01, were detected during the second period of the campaign (i.e. later than May 17th, 2023) when 16 cylinders were used. We fit a Gaussian profile to the de-dispersed FRB spectrum, integrated over the burst profile, and found that the full width at half maximum of all bursts are compatible with the 16 MHz bandwidth, apart from B14, whose extensions is only ~ 6 MHz. Furthermore, we found no evidence of scattering and sub-burst structures on time scales larger than $138.24 \mu\text{s}$ for any of the detected burst.

Given the S/N of a burst, we computed its fluence as the product of its peak flux density F_{peak} and its FWHM duration w , where the former is obtained as ([Lorimer & Kramer 2004](#)):

$$F_{\text{peak}} = S/N \frac{\text{SEFD}}{A \sqrt{N_p N_c} (1 - \xi) \Delta\nu_{\text{ch}} w} \zeta(\text{ToA}). \quad (1)$$

Here, $\text{SEFD} = 8000 \text{ Jy}$ ([Trudu et al. 2022](#)) holds for each receiver (i.e., each group of sixteen dipoles), $N_p = 1$ is the number of polarizations, $N_c = 1024$ is the number of spectral channels and $\Delta\nu_{\text{ch}} = 14.4 \text{ kHz}$ the channel width. Furthermore, A is the number of receivers included in either the eight ($A = 32$) or sixteen ($A = 64$) cylinders, ξ is the fraction of channels excised by RFIs, and, finally, the attenuation of the primary beam at the burst ToA is given by $\zeta(\text{ToA})$ ([Trudu et al. 2022](#); [Pellicciari et al. 2023](#)).

Given the burst fluence, we computed the corresponding burst spectral energy E_ν :

$$E_\nu = 10^{30} \frac{4\pi}{(1+z)^2} \left(\frac{D_L}{10^{28} \text{ cm}} \right)^2 \left(\frac{\mathcal{F}}{\text{Jy ms}} \right) \text{ erg Hz}^{-1}, \quad (2)$$

i.e., as the burst isotropic energy E_i (e.g. [Macquart & Ekers 2018](#); [Chawla et al. 2022](#)) per unit bandwidth. Here $D_L =$

380.86 Mpc is the luminosity distance of the source, obtained considering $z = 0.0771$, the redshift of the source, and the Planck 2015 cosmology ([Planck Collaboration et al. 2016](#)).

If we consider the second part of the observing campaign (at its best sensitivity), we detected 15 bursts at 408 MHz over 108 hr of on-source time, with a 10σ fluence limit of $\mathcal{F} \geq 20 \text{ Jy ms}$ ³, is $0.14 \pm 0.04 \text{ hr}^{-1}$ at 1σ confidence level. No burst showed a 1.4 GHz counterpart and we placed a 95% C.L. upper limit (UL) of 0.017 hr^{-1} on the burst rate at 1.4 GHz for fluences $\mathcal{F} \geq 13 \text{ Jy ms}$ (corresponding to $E_\nu = 2.5 \times 10^{30} \text{ erg Hz}^{-1}$).

We also computed the cumulative spectral energy rate $R(> E_\nu)$ at 408 MHz. We plotted it in Fig. 4, together with spectral energies from literature observations⁴. It follows a power law in the $3 \times 10^{30} < E_\nu < 3 \times 10^{31} \text{ erg Hz}^{-1}$ range:

$$R(> E_\nu) = R_0(> E_{\nu,0}) \left(\frac{E_\nu}{E_{\nu,0}} \right)^{\alpha_E}, \quad (3)$$

where $E_{\nu,0} = 3 \times 10^{30} \text{ erg Hz}^{-1}$. As a reference, the 20 Jy ms fluence limit of NC corresponds to $3.2 \times 10^{30} \text{ erg Hz}^{-1}$. We found the best fit values to be $R_0 = 0.25 \pm 0.07 \text{ hr}^{-1}$ and $\alpha_E = -1.5 \pm 0.3$, respectively.

We repeated the analysis for FRB 20201124A⁵, another very actively repeating FRB source ([Xu et al. 2022](#); [Zhang et al. 2022](#)). The resulting distributions are shown in Fig. 4, while the best fit parameters obtained for each observation are listed in Table 2.

The cumulative spectral energy rates are fairly similar between FRBs 20220912A and 20201124A, both in energetic and repetition rate range. This could be an indication that these two sources share the same emission mechanism ([James et al. 2020](#)), as also highlighted by other similarities such their reported double-peaked waiting time distribution and complex time-frequency structures of their bursts (see e.g. [Zhang et al. 2022, 2023](#)). Regarding FRB 20220912A, the repetition rate for bursts having $E_\nu \geq 2 \times 10^{30} \text{ erg Hz}^{-1}$ decreased from $\sim 10 \text{ hr}^{-1}$ ([Zhang et al. 2023](#); [Feng et al. 2023](#)) during a storm event, to $\sim 0.1 \text{ hr}^{-1}$, approximately 2 months later ([Sheikh et al. 2023](#)), when the storm has finished. Lastly, it dropped to less than 0.017 hr^{-1} nearly a year later, as resulting from our 1.4 GHz monitoring (see Fig. 4). However, the source remained active at 408 MHz, exhibiting comparable levels of repetition rate to those reported by [Sheikh et al. \(2023\)](#). FRB 20220912A is, as far as we know, the only FRB source that shows a decline of more than 4 orders of magnitude in its burst rate at L-band.

A similar behaviour, but inverted in frequency, can be seen for FRB 20201124A, in which the burst rate dropped from $\sim 0.2 \text{ hr}^{-1}$ as reported at 550 – 750 MHz observations ([Marthi et al. 2022](#)) to $< 5 \times 10^{-3} \text{ hr}^{-1}$ at $(2 \times 10^{31} \text{ erg Hz}^{-1})$, as resulting from non-detections at 334 MHz in $\sim 650 \text{ hr}$ of observing time ([Kirsten et al. 2024](#)). To obtain the minimum spectral energy corresponding to the latter observational campaign, we used Eq. 2, considering a 91 Jy ms completeness fluence as reported in [Kirsten et al. \(2024\)](#).

Interestingly, we note the same flattening of the cumulative spectral energy rate distribution for high energetic bursts as the one already reported for R1 ([Hewitt et al. 2022](#); [Jahns et al. 2023](#)) and recently for FRB 20201124A ([Kirsten et al. 2024](#)). As can

³ This fluence limit is obtained considering a reference burst duration of 1 ms.

⁴ Isotropic energies are obtained by multiplying the spectral energies for 16 MHz at 408 MHz and 64 MHz at 1.4 GHz, respectively.

⁵ We considered a redshift $z = 0.098$ ([Kilpatrick et al. 2021](#)), corresponding to a luminosity distance $D_L = 453.3 \text{ Mpc}$ ([Zhang et al. 2022](#)).

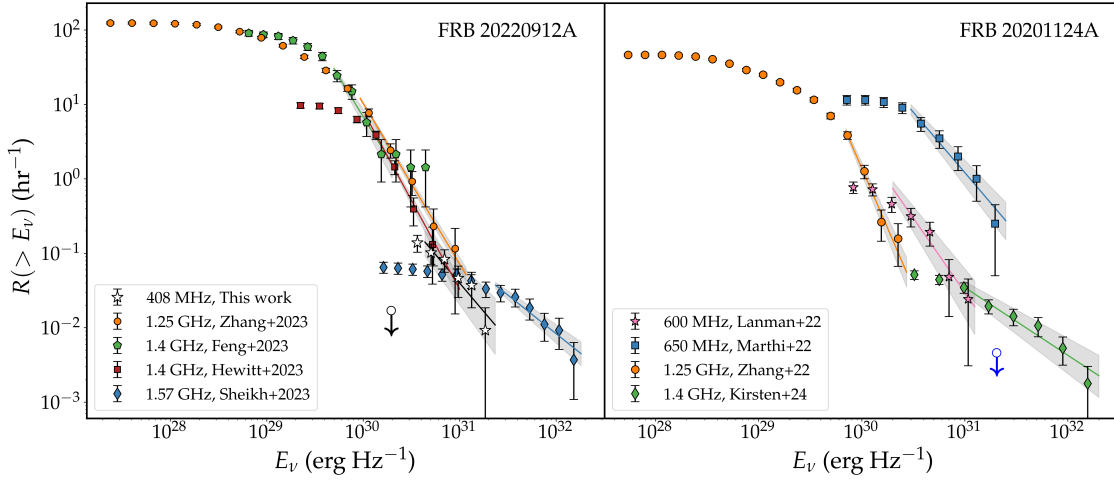


Fig. 4: Comparison between the cumulative spectral energy rate distribution for two hyperactive repeaters at different observing frequencies and times. Left: FRB 20220912A at 408 MHz (white stars; this work), 1.25 GHz (orange circles; Zhang et al. 2023), 1.4 GHz (green pentagons and red squares; Feng et al. 2023; Hewitt et al. 2023b) and 1.572 GHz (blue diamonds; Sheikh et al. 2023). The 95% C.L. UL for $R(E_v > 2.5 \times 10^{30} \text{ erg Hz}^{-1})$ from our 1.4 GHz observations is plotted as a black downward arrow. Right: FRB 20201124A at 600 MHz (pink stars; Lanman et al. 2022), 650 MHz (blue squares; Marthi et al. 2022), 1.25 GHz (orange circles; Zhang et al. 2022) and 1.4 GHz (green diamonds; Kirsten et al. 2024). The 95% C.L. UL for $R(E_v > 2 \times 10^{31} \text{ erg Hz}^{-1})$ from P (334 MHz) resulting from non-detections in Kirsten et al. (2024), is plotted as a blue downward arrows.

be noted also from the best fit values obtained for α_E in Table 2, the case for FRB 20220912A is particularly similar to FRB 20201124A. We note that α_E shifts from approximately -2 for $E_v \geq 10^{30} \text{ erg Hz}^{-1}$ to roughly -1 at $E_v \approx 2 \times 10^{31} \text{ erg Hz}^{-1}$. Moreover, high energetic bursts present a slope $\alpha_E = -1.03 \pm 0.3$, obtained by analysing L-band data from Sheikh et al. (2023), which is well consistent with the power law slope, α_E , obtained by fitting the cumulative luminosity distribution of apparently non-repeating FRBs (James et al. 2022a,b; Shin et al. 2023). As a reference, James et al. (2022a) obtained $\alpha_E = -0.95^{+0.18}_{-0.15}$, but the other measurements are still consistent with this value. Regarding R1, the cumulative isotropic energy distribution flattens to $\alpha_E = -0.88 \pm 0.01$ for $E_{\text{iso}} \geq 1.3 \times 10^{38} \text{ erg}$ (Jahns et al. 2023). This value for α roughly agrees with other reported values as obtained by fitting the R1 cumulative energy distribution at high energies (Law et al. 2017; Gourdji et al. 2019; Cruces et al. 2021; Hewitt et al. 2022). Even if the cumulative slopes are similar to the case of FRBs 20220912A and 20201124A, we note that $E_{\text{iso}} = 1.3 \times 10^{38} \text{ erg}$ corresponds to a spectral energy of $E_v \sim 4 \times 10^{29} \text{ erg Hz}^{-1}$ which is approximately 1 order of magnitude lower than the break spectral energy we obtained for the other two repeaters.

3.1. Constraints on broadband spectral index

No multi-band observations of FRB 20220912A have been reported yet. However, from a period of burst storm detected by the Five-hundred-meter Aperture Spherical Telescope (FAST), Zhang et al. (2023) obtained a synthetic L-band (1 – 1.5 GHz) spectral index of -2.6 ± 0.21 (Zhang et al. 2023). This value was obtained by fitting a spectrum obtained by averaging the fluence of all their reported bursts, characterised by having single narrow-band spectra with emission occurring only over 20%

of the observing bandwidth (Zhang et al. 2023), in different frequency channels. Although this is a valid way to obtain an in-band spectral index, we suggest some caution in a direct comparison between an UL on the global spectral index and the in-band β value obtained in Zhang et al. (2023). Indeed, our observations probe the global spectrum of the source, which can be obtained only when considering simultaneous bursts arriving at separate frequency bands.

During our observational campaign, a total of 6 bursts (B08–B13) have been detected at P-band during simultaneous L-band observations of which we do not report any counterpart. Henceforth, we use these non-detections to provide upper limits on the L-band fluence of these bursts, which in turn imply ULs on the FRB 20220912A broadband (408 MHz – 1.4 GHz) spectral index. For each detected burst with an L-band simultaneous observation we computed the fluence UL using the radiometer Eq. (1), considering the same width of the corresponding burst at P-band. We considered a 2σ detection threshold in this case since we are not searching bursts blindly with HEIMDALL, which has a minimum S/N search of ~ 6 . Instead, we inspected manually the Medicina data at burst topocentric arrival times, after correcting them for the DM of the bursts. The brightest burst we detected during our campaign is B11, with a measured fluence $F = 145 \pm 4.6 \text{ Jy ms}$ at 408 MHz. We do not report any significant radio emission down to 2σ at 1.4 GHz, and this translates into a fluence UL of 10.1 Jy ms at L-band for a burst having 14.6 ms duration. This UL translates into $\beta < -2.3$. The same limit on β is obtained by the non-detection of an L-band counterpart of B12, which has a high S/N as well but with a $\times 10$ shorter duration than B11. We report all the ULs obtained from our observations in Table 3.

Our non-detections at L-band discard the hypothesis of a positive - or flat - global spectral radio emission. We find our UL on β in disagreement with $\beta = 2.1$ as measured for a burst from R1 in a multifrequency, Arecibo (1.4 GHz) – VLA (3 GHz) campaign, i.e. the only simultaneous FRB detection present in the literature (Law et al. 2017). The other bursts reported in Law

⁶ We divided the break isotropic energy as reported in Jahns et al. (2023) by 450 MHz, i.e. an average effective bandwidth as reported therein. This value for the break spectral energy agrees well with what reported in Hewitt et al. (2022), when considering a bandwidth of 275 MHz.

Table 2: Parameters obtained from the power-law fitting of the cumulative energy distributions for FRBs 20220912A and 20201124A.

$E_{\nu,0}$ (10^{30} erg Hz $^{-1}$)	R_0 (hr $^{-1}$)	α_E	Ref.
FRB 20220912A			
1	20.5 ± 3	-2.13 ± 0.3	Feng et al. (2023)
1	10.5 ± 1.5	-2.15 ± 0.01	Zhang et al. (2023)
2	1.51 ± 0.2	-2.4 ± 0.2	Hewitt et al. (2023b)
3	0.25 ± 0.07	-1.5 ± 0.3	This work
25	0.036 ± 0.007	-1.03 ± 0.3	Sheikh et al. (2023)
FRB 20201124A			
0.5	6.8 ± 0.5	-2.5 ± 0.2	Zhang et al. (2022)
2	0.74 ± 0.18	-2.0 ± 0.3	Lanman et al. (2022)
3	9 ± 2	-1.7 ± 0.3	Marthi et al. (2022)
10	0.035 ± 0.01	-0.96 ± 0.2	Kirsten et al. (2024)

Notes. The first column represents the spectral energy threshold over which data no longer follow a simple power law, the second and third column represent the best-fit values for the parameters of the fitting power-law function (Eq. 3). The references for the data that we used to compute the cumulative burst rate distributions are listed in the last column.

Table 3: ULs on fluence and broadband spectral index β for Medicina observations for which there is a simultaneous burst detection at 408 MHz from NC radio telescope.

Burst ID	$\mathcal{F}_{1.4}$ (2σ , Jy ms)	β
B08	< 6.3	< -1.6
B09	< 4.9	< -1.4
B10	< 4.8	< -1.1
B11	< 10.1	< -2.3
B12	< 4.4	< -2.3
B13	< 5.5	< -1.9

Notes. The second and third columns represent the limits on fluence and broadband spectral index, respectively. The former represent the 2σ detection threshold, where σ is the Medicina rms noise computed on a sample of data of duration τ , with τ the FWHM of the given burst as observed at 408 MHz.

et al. (2017) have not been detected simultaneously by the two observatories, showing that the broadband spectral behaviour of the source cannot simply be modeled by a power law function. Moreover, also a spectrum with $\beta \sim 1$ as the one measured from FRB 20200428, the Galactic FRB, simultaneously detected by CHIME/FRB Collaboration et al. (2020) (400 MHz – 800 MHz) and the Survey for Transient Astronomical Radio Emission 2 (STARE-2, 1.4 GHz Bochenek et al. 2020) can be ruled out by our observations. Therefore, our upper limit could imply either that FRB 20220912A is characterised by a steep radio spectrum, or it could be a consequence of its intrinsically narrow-band emission (Zhang et al. 2023; Feng et al. 2023; Sheikh et al. 2023).

Our UL is somewhat inconsistent with the very flat spectrum usually observed for radio-loud magnetars (Camilo et al. 2008; Lazaridis et al. 2008; Dai et al. 2019). An interesting exception is the radio-loud magnetar Swift J1818.0–1607, which showed emission in a steep spectrum with $\beta \simeq -2.26$ (Lower et al. 2022). A broadband emission with this spectral index seems to be disfavoured by our observations. Nevertheless, one has to be careful in comparing the spectral index for radio-loud magnetars and FRBs, since up to now the former showed only pulsed emission (but see also Esposito et al. 2020). The only two exceptions, to date, are SGR J1935+2154 (CHIME/FRB Collaboration et al. 2020; Bochenek et al. 2020; Zhang et al. 2020;

Kirsten et al. 2021; Good & CHIME/FRB Collaboration 2020) and 1E 1547.0–5408 (Israel et al. 2021) who showed also FRB-like bursts, before entering a pulsar-like phase (Zhu et al. 2023). For the former, FRB-like bursts are emitted in random phases, unlike radio pulsations, which instead arrive in a phase windows anti-aligned with X-ray pulsations, hinting for a different emission mechanisms between radio pulses and FRB-like bursts (Zhu et al. 2023). For 1E 1547.0–5408, instead, FRB-like bursts are not aligned in phase neither with radio pulsations nor with X-ray bursts (Israel et al. 2021).

3.2. Continuum radio emission from FRB 20220912A host galaxy

In our uGMRT image at 1.26 GHz, we detect a continuum source spatially coincident with the coordinates of PSO J347.2702+48.7066, the host galaxy of FRB 20220912A. The source integrated and peak flux densities are consistent at 1σ level, so we consider it as unresolved in our observations. Its centroid have coordinates R.A. (J2000) = $23^{\text{h}}09^{\text{m}}04.88^{\text{s}} \pm 0.017^{\text{s}}$, Dec. (J2000) = $+48^{\circ}42'24.04'' \pm 0.25''$. Such position is well in agreement with R.A. (J2000) = $23^{\text{h}}09^{\text{m}}04.8988^{\text{s}} \pm 0.0003^{\text{s}}$, Dec. (J2000) = $+48^{\circ}42'23.9078'' \pm 0.005''$, i.e. the localisation of FRB 20220912A obtained from European VLBI Network (EVN) observations (Hewitt et al. 2023b). The radio contours of the source we detect are shown in Fig. 5, as well as the VLBI localisation of the FRB. In the same figure, the optical image taken from the Panoramic Survey Telescope & Rapid Response System (Pan-STARRS) data archive 1 (PS1; Flewelling et al. 2020) is shown.

We measure a flux density of $240 \pm 36 \mu\text{Jy}$ at 1.26 GHz, which corresponds to a spectral luminosity of $L_{\nu} \simeq 4 \times 10^{28}$ erg s $^{-1}$ Hz $^{-1}$. We are aware that EVN observations ruled out the presence of a PRS surrounding FRB 20220912A at milliarcsecond scale, placing an UL of 1.2×10^{28} erg s $^{-1}$ Hz $^{-1}$ on its spectral luminosity at 1.4 GHz (Hewitt et al. 2023b). In the same work, a continuum radio source, APTF J230904+484222 (APTF J23), detected by the Westerbork Synthesis Radio Telescope Aperture Tile In Focus (WSRT-APTIF) has been reported, with a position consistent with the coordinates of FRB 20220912A host galaxy. This source has a peak flux density of $270 \pm 40 \mu\text{Jy beam}^{-1}$, which falls within the measured flux range of our source, considering the associated uncertainties. Although

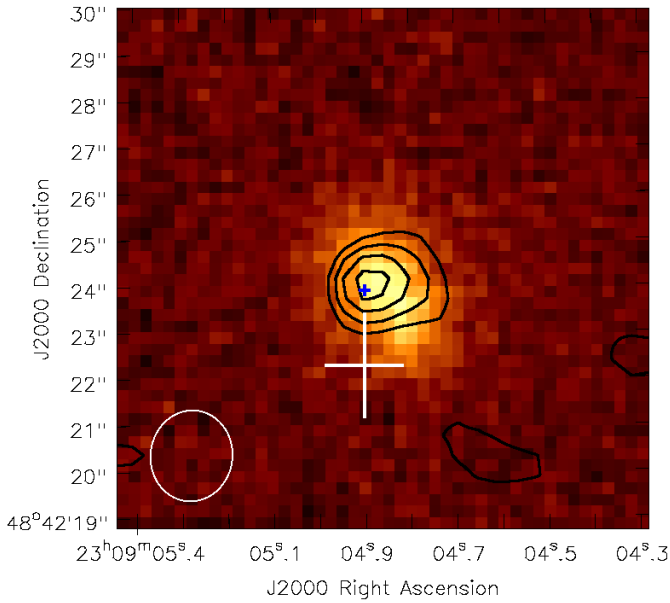


Fig. 5: Optical Pan-STARRS (i filter) image of PSO J347.2702+48.7066, the host galaxy of FRB 20220912A, with contour levels representing the continuum radio source we detected at 1.26 GHz, with a $1.97'' \times 1.77''$ synthesized beam. Contours are drawn from 3 to 6 times the rms noise level $\sigma \approx 36 \mu\text{Jy beam}^{-1}$. The white cross represents the position of APTF J23 radio source, with the cross extensions being the 1σ uncertainties on its centroid (Hewitt et al. 2023b), while the blue cross indicates the position of FRB 20220912A localised at milliarcsecond angular resolution (Hewitt et al. 2023b). The synthesized beam of our uGMRT observations is represented in the bottom left corner of the image as a white ellipse.

APTF J23 is offset by $\sim 1.6''$ with respect to the FRB VLBI position (see Fig. 5), the $\sim 2''$ uncertainties associated to its centroid makes APTF J23 consistent at 2σ level with the position of our detected source. We thus conclude that the source we detect and APTF J23 are the same radio source, albeit observed in this work with a $4\times$ better spatial resolution.

Finally, we note that the contour levels of the persistent radio source we are detecting are offset by approximately $0.6''$ (about 0.9 kpc in physical size) from the geometric centre of the host galaxy. This offset lowers the plausibility that an active galactic nucleus (AGN) is the origin of this source and, instead, suggests that the radio emission is originating from a star formation region in the vicinity of FRB 20220912A.

3.3. Results from the high energy monitoring of FRB 20220912A

We checked as a first step the bursts exposure in the AGILE source monitoring, and the position of the source within the AGILE FoV at each burst time. The relative AGILE exposure to the source is reported in Table 4. We obtained a coverage of three of the observed bursts with MCAL data but no detection was found analyzing the light curves in 5 binnings (16, 32, 64, 256 ms, and 1 s) and considering shifts of 1/4 of bin (4 shifts for the first two time scales, 2 for the second two). We extracted 3σ C.L. fluence ULs in 0.4 – 30 MeV energy band considering a cut-off power-law model with photon index -0.70 and cut-off energy 65 keV (as reported for the FRB 200428 burst by Mereghetti et al.

2020). We also estimated UL fluences which would be required to issue a trigger with the onboard 1 ms MCAL trigger logic timescale (see Ursi et al. 2022b). We report the corresponding ULs in Table 4. The most stringent UL that we can place on the radio efficiency $\eta = E_\gamma/E_{\text{Radio}}$ is from burst B05, for which the non-activation of the MCAL trigger system permits to obtain $\eta < 1.5 \times 10^9$ in the 0.4 – 30 MeV energy range. We note that this UL for η is conservative. Indeed, η depends on the radio isotropic energy of the burst, which in turn relies on the spectral occupancy. In our case, we considered $\Delta\nu = 16$ MHz, which is the observed bandwidth of the NC radio telescope, but the intrinsic spectral extension of the burst likely exceeds this value, giving tighter constraints on η .

AGILE/GRID covered 2 of the 16 bursts (B05 and B15) at their ToA. We analyzed GRID data near burst arrival times on short (100 s around the bursts), and longer timescales (± 10 days and 100 days starting about B05 trigger time). The long-timescale data analysis was performed applying the standard AGILE multi-source maximum likelihood (AML; Bulgarelli et al. 2012), which is mainly applied to exposures longer than a few hours. We report no detection at short timescales for AGILE/GRID. Finally, we extracted 3σ ULs in the $E \geq 100$ MeV band for two long time integrations, 10 days after each burst and 100 days after burst B05 (the latter period of time includes also B15). We obtained $\text{UL}_{10d} = 2.0 \times 10^{-11} \text{ erg cm}^{-2} \text{ s}^{-1}$ and $\text{UL}_{100d} = 4.4 \times 10^{-12} \text{ erg cm}^{-2} \text{ s}^{-1}$. From the latter, we obtain $L_\gamma < 7.1 \times 10^{43} \text{ erg s}^{-1}$ for the persistent γ -ray luminosity of the source.

No X-ray source was detected at $> 3\sigma$ C.L. in the whole Swift/XRT WT mode dataset. We note however, with a detailed single observation check, that no radio burst was exposed even including three more proposals acquired in photon counting (PC) mode: burst B01 occurred 16 hrs after the observation on October 16th, 2022, and B16 occurred within our third observations but did not fall within the WT mode sky window. We then extracted 3σ countrate ULs for our observations using the XIMAGE package (sosta command) and converted to fluxes using a standard single power-law spectral model with a photon index of 2.0, and correcting for absorption for a column density N_H fixed to the Galactic value of $1.43 \times 10^{21} \text{ cm}^{-2}$ (HI4PI Collaboration et al. 2016) redshifted for the redshift of the source (Ravi et al. 2023). The X-ray observations exposure and the corresponding ULs for the persistent X-ray fluence are reported in Table 5. From the latter, we obtain an UL for the persistent X-ray luminosity $L_X = 4\pi D_L^2 F_X / (1+z) < 3.4 \times 10^{42} \text{ erg s}^{-1}$, where D_L is the luminosity distance of FRB 20220912A. We note that this UL excludes the majority of mid and high luminosity AGN, which typically have X-ray luminosity $L_X \geq 10^{43} \text{ erg s}^{-1}$ (e.g. Padovani et al. 2017). This brings further evidence that the radio source detected with uGMRT (see Section 3.2) originates from a region of star formation, rather than from an AGN.

4. Summary and conclusions

In this work we presented a campaign of simultaneous observations at 408 MHz and 1.4 GHz, taken with the NC and Mc radiotelescopes, respectively, of the repeating FRB 20220912A, one of the most active repeaters known to date. During the campaign, we detected 16 bursts from FRB 20220912A at 408 MHz for a limiting 10σ fluence $\mathcal{F} \geq 20 \text{ Jy ms}$. We found that the cumulative burst rate as a function of the spectral energy at 408 MHz can be well fitted with a single power law function $R(> E_\nu) \propto E_\nu^{\alpha_E}$, with $\alpha_E = -1.5 \pm 0.3$. We do not report any burst detection at 1.4 GHz in a total of 177 hr above a S/N = 10,

Table 4: AGILE FRB 20220912A bursts coverage and MCAL ULs.

Burst ID	MCAL FoV	MCAL D.A.	GRID FoV	UL (3 σ) [erg cm ⁻²]	MCAL trigger FAR [evt/hour]	UL 1 ms [erg cm ⁻²]
B01				idle mode		
B02	YES	NO	NO	–	–	3.22×10^{-8}
B03				idle mode		
B04	YES	NO	NO	–	–	2.59×10^{-8}
B05	YES	NO	YES	–	–	1.84×10^{-8}
B06	YES	NO	NO	–	–	5.15×10^{-8}
B07				no data		
B08	YES	NO	NO	–	–	4.22×10^{-8}
B09	YES	YES	NO	2.06×10^{-7}	~ 4.0	–
B10	YES	YES	NO	2.04×10^{-7}	~ 4.0	–
B11	YES	YES	NO	2.00×10^{-7}	~ 4.0	–
B12	YES	NO	NO	–	–	2.17×10^{-8}
B13				idle mode		
B14				idle mode		
B15	YES	NO	YES	–	–	1.83×10^{-8}
B16				no data		

Notes. The second and fourth columns report the presence or absence of the source in the field of view (FoV) of the two onboard detectors here considered, respectively. In the third column we report the existence of an MCAL data acquisition at trigger time. MCAL fluence 3 σ ULs in 0.4–30 MeV band are evaluated only when no coincident data acquisitions at the burst times is present; MCAL trigger "False Alarm Rate" (FAR) are evaluated when coincident data acquisition is present. ULs (1 ms) refer to the UL fluences that would be required to issue a trigger with the onboard 1 ms MCAL trigger logic timescale (see [Ursi et al. 2022a](#)). Since there is no evidence of a detection in the acquired triggers, we checked in the 100 days preceding each burst time to estimate the FAR corresponding to each trigger.

Table 5: Swift exposures and flux ULs (0.3–10 keV).

Start time (UTC)	Stop time	UL [erg cm ⁻² s ⁻¹]
2022-11-11 19:26:15	2022-11-20 18:29:56	2.3×10^{-13}
2023-07-25 00:09:32	2023-07-30 02:47:55	2.5×10^{-13}
2023-08-29 21:26:07	2023-09-09 21:01:56	2.1×10^{-13}
2023-09-29 22:27:14	2023-10-05 21:30:56	4.9×10^{-13}

which corresponds to a fluence and a spectral energy thresholds of $\mathcal{F} \geq 13$ Jy ms and 2.5×10^{30} erg Hz⁻¹, respectively. These non-detections place an UL of 0.017 hr⁻¹ at 95% C.L. for the burst rate at 1.4 GHz, which is ~ 4 orders of magnitude lower than the level of activity reported at the same frequency during a burst storm of the source ([Zhang et al. 2023](#); [Feng et al. 2023](#)) at the same spectral energy. On the other hand, the source remained active at 408 MHz with comparable repetition rate as observed from a long monitoring after the end of the burst storm ([Sheikh et al. 2023](#)). Interestingly, we note that the cumulative spectral energy rate distribution of FRB 20220912A flattens for bursts having spectral energy $E_\nu \geq 10^{31}$ erg Hz⁻¹, changing slope from approximately $\alpha_E \approx -2$ to $\alpha_E \approx -1$. This flattening feature has been reported so far for two other well-studied hyperactive repeaters, R1 ([Hewitt et al. 2022](#); [Jahns et al. 2023](#)) and FRB 20201124A ([Kirsten et al. 2024](#)). As discussed in [Kirsten et al. \(2024\)](#), this could be linked to a different type of emission mechanism, emission site or beaming angle between low and high energy bursts and could potentially represents a link between one-off bursts and repeating sources ([James et al. 2022b](#); [Kirsten et al. 2024](#)). The fact that also FRB 20220912A shows this kind of behaviour, combined with the fact that high energy bursts present a slope well consistent with that of the non-repeaters population ([James et al. 2022a,b](#); [Shin et al. 2023](#)),

provides further support to the idea that a fraction of apparently non-repeating FRBs could be, instead, repeating sources with very low repetition rates ([Ravi 2019](#); [James 2023](#)). We compared the cumulative spectral energy rate for FRB 20220912A and FRB 20201124A, highlighting a strong similarity between the two distributions, both in terms of spectral energy and repetition rate range.

In total, 6 of the 16 bursts detected at 408 MHz arrived during simultaneous observations at 1.4 GHz, allowing us to place the first ULs to the broadband (408 MHz – 1.4 GHz) spectral index β of FRB 20220912A. Analyzing Mc data at the ToA of burst B11, which has the highest fluence, we obtained an UL of $\beta < -2.3$, indicating that the source, under the assumption of an intrinsically broadband emission, exhibits a very steep spectral index. Our observations then strongly disfavor a flat or even inverted spectrum for FRB 20220912A. We note that this is different than what has been reported for the only two simultaneous detections of FRBs in separate frequency bands, the latter indicating a positive spectral index ([Law et al. 2017](#); [Bochenek et al. 2020](#); [CHIME/FRB Collaboration et al. 2020](#)). Our findings supports the idea that the intrinsic spectrum of FRB 20220912A is narrow-band, as reported in recent observations ([Zhang et al. 2023](#); [Feng et al. 2023](#); [Sheikh et al. 2023](#); [Hewitt et al. 2023b](#)).

Additionally, we reported 3 hr long continuum radio observations of FRB 20220912A field using the band-5 (1050 – 1450 MHz) of the uGMRT. We detected a continuum radio source of $240 \pm 40 \mu\text{Jy}$ flux density, spatially coincident with the FRB 20220912A VLBI localisation. As being not detected in recent, deep, EVN observations (Hewitt et al. 2023b), we suggest that this continuum radio source is possibly originating from a region of star formation, potentially located in the vicinity of the FRB source. This is corroborated by the $0.6''$ offset (0.9 kpc in physical size) between the source centroid and the geometric centre of the optical host galaxy, which excludes the hypothesis that the radio source is being powered by an AGN.

Finally, we also reported results of an X- and γ -ray monitoring of FRB 20220912A with the Swift and AGILE space missions at X- and γ rays, respectively. We reported no detection for both the high energy campaigns. Regarding AGILE, we place an UL on the radio efficiency of $\eta = E_\gamma/E_{\text{radio}} < 1.5 \times 10^9$ for the B05 burst and a persistent γ -ray luminosity UL of $L_\gamma < 7.1 \times 10^{43} \text{ erg s}^{-1}$. From Swift observations we obtained instead an UL for the persistent X-ray luminosity (0.3 – 10 keV) of $L_X < 3.4 \times 10^{42} \text{ erg s}^{-1}$.

Acknowledgements. The reported data were collected during the phase of the INAF scientific exploitation with the NC radio telescope.

References

- Agarwal, D., Aggarwal, K., Burke-Spolaor, S., Lorimer, D. R., & Garver-Daniels, N. 2020, MNRAS, 497, 1661, doi: [10.1093/mnras/staa1856](#)
- Anna-Thomas, R., Connor, L., Dai, S., et al. 2023, Science, 380, 599, doi: [10.1126/science.abo6526](#)
- Bailes, M. 2022, Science, 378, abj3043, doi: [10.1126/science.abj3043](#)
- Barsdell, B. R., Bailes, M., Barnes, D. G., & Fluke, C. J. 2012, MNRAS, 422, 379, doi: [10.1111/j.1365-2966.2012.20622.x](#)
- Beloborodov, A. M. 2020, ApJ, 896, 142, doi: [10.3847/1538-4357/ab83eb](#)
- Bhandari, S., Marcote, B., Sridhar, N., et al. 2023, ApJ, 958, L19, doi: [10.3847/2041-8213/ad083f](#)
- Bochenek, C. D., Ravi, V., Belov, K. V., et al. 2020, Nature, 587, 59, doi: [10.1038/s41586-020-2872-x](#)
- Bochenek, C. D., Ravi, V., & Dong, D. 2021, ApJ, 907, L31, doi: [10.3847/2041-8213/abd634](#)
- Bulgarelli, A., Chen, A. W., Tavani, M., et al. 2012, A&A, 540, A79, doi: [10.1051/0004-6361/201118023](#)
- Burke-Spolaor, S., Trott, C. M., Brisken, W. F., et al. 2016, ApJ, 826, 223, doi: [10.3847/0004-637X/826/2/223](#)
- Burrows, D. N., Hill, J. E., Nousek, J. A., et al. 2005, Space Sci. Rev., 120, 165, doi: [10.1007/s11214-005-5097-2](#)
- Camilo, F., Reynolds, J., Johnston, S., Halpern, J. P., & Ransom, S. M. 2008, ApJ, 679, 681, doi: [10.1086/587054](#)
- Chatterjee, S., Law, C. J., Wharton, R. S., et al. 2017, Nature, 541, 58, doi: [10.1038/nature20797](#)
- Chawla, P., Andersen, B. C., Bhardwaj, M., et al. 2020, ApJ, 896, L41, doi: [10.3847/2041-8213/ab96bf](#)
- Chawla, P., Kaspi, V. M., Ransom, S. M., et al. 2022, ApJ, 927, 35, doi: [10.3847/1538-4357/ac49e1](#)
- CHIME Collaboration, Amiri, M., Bandura, K., et al. 2022, ApJS, 261, 29, doi: [10.3847/1538-4365/ac6fd9](#)
- CHIME/FRB Collaboration, Andersen, B. C., Bandura, K. M., et al. 2020, Nature, 587, 54, doi: [10.1038/s41586-020-2863-y](#)
- CHIME/FRB Collaboration, Amiri, M., Andersen, B. C., et al. 2021, ApJS, 257, 59, doi: [10.3847/1538-4365/ac33ab](#)
- CHIME/FRB Collaboration, Andersen, B. C., Bandura, K., et al. 2023, ApJ, 947, 83, doi: [10.3847/1538-4357/acc6c1](#)
- Cruces, M., Spitler, L. G., Scholz, P., et al. 2021, MNRAS, 500, 448, doi: [10.1093/mnras/staa3223](#)
- Dai, S., Lower, M. E., Bailes, M., et al. 2019, ApJ, 874, L14, doi: [10.3847/2041-8213/ab0e7a](#)
- Duncan, R. C., & Thompson, C. 1992, ApJ, 392, L9, doi: [10.1086/186413](#)
- Esposito, P., Rea, N., Borghese, A., et al. 2020, ApJ, 896, L30, doi: [10.3847/2041-8213/ab9742](#)
- Feng, Y., Li, D., Zhang, Y.-K., et al. 2023, arXiv e-prints, arXiv:2304.14671, doi: [10.48550/arXiv.2304.14671](#)
- Flewelling, H. A., Magnier, E. A., Chambers, K. C., et al. 2020, ApJS, 251, 7, doi: [10.3847/1538-4365/abb82d](#)
- Gajjar, V., Siemion, A. P. V., Price, D. C., et al. 2018, ApJ, 863, 2, doi: [10.3847/1538-4357/aad005](#)
- Gehrels, N., Chincarini, G., Giommi, P., et al. 2004, ApJ, 611, 1005, doi: [10.1086/422091](#)
- Good, D., & CHIME/FRB Collaboration. 2020, The Astronomer's Telegram, 14074, 1
- Gordon, A. C., Fong, W.-f., Kilpatrick, C. D., et al. 2023, ApJ, 954, 80, doi: [10.3847/1538-4357/ace5aa](#)
- Gourdji, K., Michilli, D., Spitler, L. G., et al. 2019, ApJ, 877, L19, doi: [10.3847/2041-8213/ab1f8a](#)
- Hessels, J. W. T., Spitler, L. G., Seymour, A. D., et al. 2019, ApJ, 876, L23, doi: [10.3847/2041-8213/ab13ae](#)
- Hewitt, D. M., Snelders, M. P., Hessels, J. W. T., et al. 2022, MNRAS, 515, 3577, doi: [10.1093/mnras/stac1960](#)
- Hewitt, D. M., Hessels, J. W. T., Ould-Boukattine, O. S., et al. 2023a, arXiv e-prints, arXiv:2308.12118, doi: [10.48550/arXiv.2308.12118](#)
- Hewitt, D. M., Bhandari, S., Marcote, B., et al. 2023b, arXiv e-prints, arXiv:2312.14490, doi: [10.48550/arXiv.2312.14490](#)
- HI4PI Collaboration, Ben Bekhti, N., Flöer, L., et al. 2016, A&A, 594, A116, doi: [10.1051/0004-6361/201629178](#)
- Israel, G. L., Burgay, M., Rea, N., et al. 2021, ApJ, 907, 7, doi: [10.3847/1538-4357/abca95](#)
- Jahns, J. N., Spitler, L. G., Nimmo, K., et al. 2023, MNRAS, 519, 666, doi: [10.1093/mnras/stac3446](#)
- James, C. W. 2023, PASA, 40, e057, doi: [10.1017/pasa.2023.51](#)
- James, C. W., Prochaska, J. X., Macquart, J. P., et al. 2022a, MNRAS, 510, L18, doi: [10.1093/mnras/rlab117](#)
- James, C. W., Osłowski, S., Flynn, C., et al. 2020, ApJ, 895, L22, doi: [10.3847/2041-8213/ab8f99](#)
- James, C. W., Ghosh, E. M., Prochaska, J. X., et al. 2022b, MNRAS, 516, 4862, doi: [10.1093/mnras/stac2524](#)
- Kilpatrick, C. D., Fong, W., Prochaska, J. X., et al. 2021, The Astronomer's Telegram, 14516, 1
- Kirsten, F., Jenkins, M., Snelders, M., et al. 2020, The Astronomer's Telegram, 13735, 1
- Kirsten, F., Snelders, M. P., Jenkins, M., et al. 2021, Nature Astronomy, 5, 414, doi: [10.1038/s41550-020-01246-3](#)
- Kirsten, F., Hessels, J. W. T., Hewitt, D. M., et al. 2022, The Astronomer's Telegram, 15727, 1
- Kirsten, F., Ould-Boukattine, O. S., Herrmann, W., et al. 2024, Nature Astronomy, doi: [10.1038/s41550-023-02153-z](#)
- Kumar, P., Shannon, R. M., Flynn, C., et al. 2021, MNRAS, 500, 2525, doi: [10.1093/mnras/staa3436](#)
- Lanman, A. E., Andersen, B. C., Chawla, P., et al. 2022, ApJ, 927, 59, doi: [10.3847/1538-4357/ac4bc7](#)
- Law, C. J., Abruzzo, M. W., Bassa, C. G., et al. 2017, ApJ, 850, 76, doi: [10.3847/1538-4357/aa9700](#)
- Lazaridis, K., Jessner, A., Kramer, M., et al. 2008, MNRAS, 390, 839, doi: [10.1111/j.1365-2966.2008.13794.x](#)
- Li, D., Wang, P., Zhu, W. W., et al. 2021, Nature, 598, 267, doi: [10.1038/s41586-021-03878-5](#)
- Locatelli, N. T., Bernardi, G., Bianchi, G., et al. 2020, MNRAS, 494, 1229, doi: [10.1093/mnras/staa813](#)
- Lorimer, D. R. 2011, SIGPROC: Pulsar Signal Processing Programs, Astrophysics Source Code Library, record ascl:1107.016
- Lorimer, D. R., & Kramer, M. 2004, Handbook of Pulsar Astronomy, Vol. 4
- Lower, M. E., Shannon, R. M., & Kumar, P. 2022, The Astronomer's Telegram, 15172, 1
- Lu, W., Kumar, P., & Zhang, B. 2020, MNRAS, 498, 1397, doi: [10.1093/mnras/staa2450](#)
- Lyubarsky, Y. 2020, ApJ, 897, 1, doi: [10.3847/1538-4357/ab97b5](#)
- Macquart, J. P., & Ekers, R. 2018, MNRAS, 480, 4211, doi: [10.1093/mnras/sty2083](#)
- Marcote, B., Kirsten, F., Hessels, J., et al. 2022, in European VLBI Network Mini-Symposium and Users' Meeting 2021, Vol. 2021, 35, doi: [10.22323/1.399.0035](#)
- Marcote, B., Paragi, Z., Hessels, J. W. T., et al. 2017, ApJ, 834, L8, doi: [10.3847/2041-8213/834/2/L8](#)
- Margalit, B., & Metzger, B. D. 2018, ApJ, 868, L4, doi: [10.3847/2041-8213/aaedad](#)
- Marthi, V. R., Bethapudi, S., Main, R. A., et al. 2022, MNRAS, 509, 2209, doi: [10.1093/mnras/stab3067](#)
- McKinnon, R., & CHIME/FRB Collaboration. 2022, The Astronomer's Telegram, 15679, 1
- McMullin, J. P., Waters, B., Schiebel, D., Young, W., & Golap, K. 2007, in Astronomical Society of the Pacific Conference Series, Vol. 376, Astronomical Data Analysis Software and Systems XVI, ed. R. A. Shaw, F. Hill, & D. J. Bell, 127

- Mereghetti, S., Savchenko, V., Ferrigno, C., et al. 2020, *ApJ*, 898, L29, doi: [10.3847/2041-8213/aba2cf](#)
- Michilli, D., Seymour, A., Hessels, J. W. T., et al. 2018, *Nature*, 553, 182, doi: [10.1038/nature25149](#)
- Nimmo, K., Hessels, J. W. T., Snelders, M. P., et al. 2022, arXiv e-prints, arXiv:2206.03759, doi: [10.48550/arXiv.2206.03759](#)
- Niu, C. H., Aggarwal, K., Li, D., et al. 2022, *Nature*, 606, 873, doi: [10.1038/s41586-022-04755-5](#)
- Padovani, P., Alexander, D. M., Assef, R. J., et al. 2017, *A&A Rev.*, 25, 2, doi: [10.1007/s00159-017-0102-9](#)
- Pastor-Marazuela, I., Connor, L., van Leeuwen, J., et al. 2021, *Nature*, 596, 505, doi: [10.1038/s41586-021-03724-8](#)
- Pellicciari, D., Bernardi, G., Pilia, M., et al. 2023, *A&A*, 674, A223, doi: [10.1051/0004-6361/202346307](#)
- Perley, R. A., & Butler, B. J. 2013, *ApJS*, 204, 19, doi: [10.1088/0067-0049/204/2/19](#)
- Petroff, E., Hessels, J. W. T., & Lorimer, D. R. 2022, *A&A Rev.*, 30, 2, doi: [10.1007/s00159-022-00139-w](#)
- Piro, L., Bruni, G., Troja, E., et al. 2021, *A&A*, 656, L15, doi: [10.1051/0004-6361/202141903](#)
- Planck Collaboration, Ade, P. A. R., Aghanim, N., et al. 2016, *A&A*, 594, A13, doi: [10.1051/0004-6361/201525830](#)
- Pleunis, Z., Good, D. C., Kaspi, V. M., et al. 2021, *ApJ*, 923, 1, doi: [10.3847/1538-4357/ac33ac](#)
- Popov, S. B., & Postnov, K. A. 2013, arXiv e-prints, arXiv:1307.4924, doi: [10.48550/arXiv.1307.4924](#)
- Rajwade, K., Wharton, R., Majid, W., et al. 2022, *The Astronomer's Telegram*, 15791, 1
- Ransom, S. M., Eikenberry, S. S., & Middleditch, J. 2002, *AJ*, 124, 1788, doi: [10.1086/342285](#)
- Ravi, V. 2019, *Nature Astronomy*, 3, 928, doi: [10.1038/s41550-019-0831-y](#)
- Ravi, V., Catha, M., Chen, G., et al. 2023, *ApJ*, 949, L3, doi: [10.3847/2041-8213/acc4b6](#)
- Resmi, L., Vink, J., & Ishwara-Chandra, C. H. 2021, *A&A*, 655, A102, doi: [10.1051/0004-6361/202039771](#)
- Ridnaia, A., Golenetskii, S., Aptekar, R., et al. 2020, *GRB Coordinates Network*, 27554, 1
- Sand, K. R., Breitman, D., Michilli, D., et al. 2023, arXiv e-prints, arXiv:2307.05839, doi: [10.48550/arXiv.2307.05839](#)
- Sheikh, S., Farah, W., Pollak, A. W., et al. 2022, *The Astronomer's Telegram*, 15735, 1
- Sheikh, S. Z., Farah, W., Pollak, A. W., et al. 2023, arXiv e-prints, arXiv:2312.07756, doi: [10.48550/arXiv.2312.07756](#)
- Shin, K., Masui, K. W., Bhardwaj, M., et al. 2023, *ApJ*, 944, 105, doi: [10.3847/1538-4357/acaf06](#)
- Sobacchi, E., Lyubarsky, Y., Beloborodov, A. M., & Sironi, L. 2022, *MNRAS*, 511, 4766, doi: [10.1093/mnras/stac251](#)
- Sridhar, N., Metzger, B. D., & Fang, K. 2024, *ApJ*, 960, 74, doi: [10.3847/1538-4357/ad03e8](#)
- Tavani, M., Barbiellini, G., Argan, A., et al. 2009, *A&A*, 502, 995, doi: [10.1051/0004-6361/200810527](#)
- Tavani, M., Verrecchia, F., Casentini, C., et al. 2020, *ApJ*, 893, L42, doi: [10.3847/2041-8213/ab86b1](#)
- Tavani, M., Casentini, C., Ursi, A., et al. 2021, *Nature Astronomy*, 5, 401, doi: [10.1038/s41550-020-01276-x](#)
- Thompson, C., & Duncan, R. C. 1995, *MNRAS*, 275, 255, doi: [10.1093/mnras/275.2.255](#)
- Trudu, M., Pilia, M., Bernardi, G., et al. 2022, *MNRAS*, 513, 1858, doi: [10.1093/mnras/stac1031](#)
- Trudu, M., Pilia, M., Nicastro, L., et al. 2023, *A&A*, 676, A17, doi: [10.1051/0004-6361/202245303](#)
- Tuccari, G. 2003, in *Astronomical Society of the Pacific Conference Series*, Vol. 306, New technologies in VLBI, ed. Y. C. Minh, 177
- Ursi, A., Verrecchia, F., Piano, G., et al. 2022a, *ApJ*, 924, 80, doi: [10.3847/1538-4357/ac332f](#)
- . 2022b, *ApJ*, 924, 80, doi: [10.3847/1538-4357/ac332f](#)
- Whitney, A., Kettenis, M., Phillips, C., & Sekido, M. 2010, in *Sixth International VLBI Service for Geodesy and Astronomy. Proceedings from the 2010 General Meeting*, ed. R. Navarro, S. Rogstad, C. E. Goodhart, E. Sigman, M. Soriano, D. Wang, L. A. White, & C. S. Jacobs, 192–196
- Xu, H., Niu, J. R., Chen, P., et al. 2022, *Nature*, 609, 685, doi: [10.1038/s41586-022-05071-8](#)
- Xu, J., Feng, Y., Li, D., et al. 2023, *Universe*, 9, 330, doi: [10.3390/universe9070330](#)
- Zhang, B. 2023, *Reviews of Modern Physics*, 95, 035005, doi: [10.1103/RevModPhys.95.035005](#)
- Zhang, C. F., Jiang, J. C., Men, Y. P., et al. 2020, *The Astronomer's Telegram*, 13699, 1
- Zhang, Y.-K., Wang, P., Feng, Y., et al. 2022, *Research in Astronomy and Astrophysics*, 22, 124002, doi: [10.1088/1674-4527/ac98f7](#)
- Zhang, Y.-K., Li, D., Zhang, B., et al. 2023, arXiv e-prints, arXiv:2304.14665, doi: [10.48550/arXiv.2304.14665](#)
- Zhou, D. J., Han, J. L., Zhang, B., et al. 2022, *Research in Astronomy and Astrophysics*, 22, 124001, doi: [10.1088/1674-4527/ac98f8](#)
- Zhu, W., Xu, H., Zhou, D., et al. 2023, *Science Advances*, 9, eadf6198, doi: [10.1126/sciadv.adf6198](#)